Journal of Applied Polymer Science

New polynomial strain energy function; application to rubbery circular cylinders under finite extension and torsion

Marzieh Bahreman, Hossein Darijani
Mechanical Engineering Department, Shahid Bahonar University of Kerman, Kerman, Iran
Correspondence to: H. Darijani (E-mail: darijani@uk.ac.ir or hdarijani@gmail.com)

ABSTRACT: In this article, a strain energy density function is proposed in terms of the principal invariants of the left Cauchy-Green strain tensor for Rubber-like materials. This model due to its mathematical structure lies in the category of polynomial hyperelastic models. To compare the performance of the proposed model with the Rivlin set, some test data of rubber-like materials with pure homogeneous deformations are used. It is shown that the proposed model has better agreement with the test data compared to the selected model. As an application of the proposed model, it is used to obtain a closed form solution for analysis of rubbery solid circular cylinders with S-shaped and semi J-shaped mechanical behavior under the torsion superimposed on the axial extension. Moreover, the results predicted from the proposed model are compared to classic models to investigate the results accuracy for simplification done. © 2014 Wiley Periodicals, Inc. J. Appl. Polym. Sci. **2015**, *132*, 41718.

KEYWORDS: elastomers; rubber; structure-property relations; theory and modeling

Received 1 July 2014; accepted 30 October 2014
DOI: 10.1002/app.41718

INTRODUCTION

To characterize the mechanical behavior of rubber-like materials, it is a common practice to represent the constitutive equation through a strain energy density function. An elastic material that has a strain energy density is known as a hyperelastic material.[1,2] Many theoretical models have been developed to characterize the mechanical behavior of hyperelastic materials. These models are divided into two categories: models based on statistical mechanics and those which take the phenomenological approach of treating the material as a continuum.[3] The statistical approach is concerned with assumed statistical distributions of the lengths, orientations, and structure of rubber molecular networks. The phenomenological approach is based on the observation of rubber under various conditions of homogeneous strain and is concerned with fitting mathematical equations to experimental data. Based on the phenomenological approach, models are invariant-based or stretch-based. For example, Mooney[4] published an invariant-based phenomenological model in terms of principal invariants of the left Cauchy-Green strain tensor. Later, Treloar[5] proposed the so-called Neo-Hookean material model in terms of the first invariant with only one material parameter. Kakavas[6] expressed the strain energy density function in terms of the second and third invariants of the logarithmic strain tensor with three material parameters. The two-parameter Gent model[7] is a first invariant-based and has some attractive features. Rivlin[8] introduced a generalized model, also called polynomial hyperelastic model, in terms of strain invariants. Following this structure, several investigators attempted to take into account strain invariants in their models in the framework of polynomial hyperelastic model. For example, Yeoh model[9] and Biderman model,[10] altogether are polynomial forms of strain energy and encompass the high order of strain invariants.

Rivlin and Saunders[11] proposed that a strain energy density function is expressible in the form of even powered series of the principal stretches. A variety of strain energy density functions have been extracted from Rivlin's model. Valanis-Landel[12] proposed that a strain energy density can be written as sum of independent functions of the principal stretches for incompressible materials. Attard[13] presented the strain energy density as a geometric series of principal stretches containing only even powers. Another important phenomenological theory is attributed to Ogden.[14] Ogden proposed that the strain energy function can be represented as a series of principal stretches with real positive and negative powers. This model gives accurate results with at least three terms.

In this article, it is considered a polynomial model with only integer even powers of stretches to give a satisfactory correspondence with experimental results over wide ranges of different types of deformation. This constitutive model is represented in terms of the first and second invariants of Cauchy-Green strain tensor **B**. It has a simple mathematical form and is appropriate to describe the

deformability of rubber-like materials at large strain levels. It is noteable that this model has a structure similar to Rivlin model. To investigate the appropriateness of this model in comparison to other polynomial-type strain energy densities specially family of Rivlin, several experimental results for incompressible materials under homogeneous strain are examined. The results are compared with those of extracted from the Rivlin model. This model can provide the foundation of existence of a closed form solution for the boundry value problems in the finite deformation elasticity. Here, as an application of this model, it is applied to the problem of torsion and extension of hyperelastic solid circular cylinders. This problem has been investigated theoretically by many researchers. Kanner and Horgan[15] investigated the effects of strain-stiffening on the response of solid circular cylinders in the combined deformation of torsion and axial extension by considering particular constitutive models for materials that reflect limiting chain extensibility at the molecular level. Horgan and Murphy[16] formulated the problem of torsion and extension of a solid circular cylinder for a general strain energy density that depends on alternative invariants, namely the invariants of the stretch tensor. In this article, the analytical solution for the problem of torsion and extension of a solid circular cylinder made of the elastomers with S-shaped and semi J-shaped mechanical behavior is derived. Moreover, the results of this solution are compared with those of extracted from classical strain energy densities, Moony-Rivlin and Neo-Hookean. These comparisons are done to investigate the application the well-known classic models instead of the presented higher-order model without loss in accuracy.

FUNDAMENTALS

We recall that the general motion of a continuum is described by $\mathbf{x}=\chi(\mathbf{X},t)$, where $\boldsymbol{x}$ is the spatial position at time t of a material particle with the material coordinate $\mathbf{X}$. χ is a vector field that specifies the place $\mathbf{x}$ of $\mathbf{X}$ for all fixed t, and is called the motion of the body. The motion χ carries points $\mathbf{X}$ located at the initial configuration to places $\mathbf{x}$ in the current configuration. The relation between d$\mathbf{X}$ and d$\mathbf{x}$ is given by[1]

$$d\mathbf{x}=F\,d\mathbf{X} \tag{1}$$

where $\mathbf{F}$ is the deformation gradient tensor and transforms a material element d$\mathbf{X}$ at the reference configuration into a material element d$\mathbf{x}$ at time t. In general, $\mathbf{F}$ has nine components for all t, and it characterizes the behavior of motion in the neighborhood of a point. Since $\det(\mathbf{F})>0$, the polar decomposition theorem states that $\mathbf{F}$ is uniquely decomposed as[1]

$$\boldsymbol{F}=\boldsymbol{RU}=\boldsymbol{VR} \tag{2}$$

where $\boldsymbol{U}$ and $\boldsymbol{V}$ are the right and left stretch tensors, respectively. $\boldsymbol{U}$ and $\boldsymbol{V}$ are positive definite symmetric tensors and $\boldsymbol{R}$ is a proper orthogonal rotation tensor, which represents the rotation of the eigenvectors of $\boldsymbol{U}$, N_i to the eigenvectors of $\boldsymbol{V}$, n_i:

$$n_i=\boldsymbol{R}\,N_i \tag{3}$$

The other measures of deformation are as follows[2]

$$\boldsymbol{C}=\boldsymbol{F}^{\mathrm{T}}\boldsymbol{F}=\boldsymbol{U}^2,\ \boldsymbol{B}=\boldsymbol{F}\boldsymbol{F}^{\mathrm{T}}=\boldsymbol{V}^2 \tag{4}$$

where $\boldsymbol{B}$ and $\boldsymbol{C}$ are the left and rigth Cauchy-Green tensors, respectively, and the symbol of supra T denotes to the transpose of tensor. Let $\lambda_1,\lambda_2,\lambda_3$ be eigenvalues of the stretch tensors. Indeed, λ_i are the principal stretches of the deformation. The strain energy density of a homogeneous, isotropic, elastic material is generally represented in terms of three independent stretch invariants. The most common invariants are[2]

$$\begin{aligned} I_1&=\mathrm{tr}(\mathbf{B})=\lambda_1^2+\lambda_2^2+\lambda_3^2\\ I_2&=\frac{1}{2}\left((\mathrm{tr}(B))^2-\mathrm{tr}(B^2)\right)=\lambda_1^2\lambda_2^2+\lambda_1^2\lambda_3^2+\lambda_2^2\lambda_3^2\\ I_3&=\det(\boldsymbol{B})=\lambda_1^2\lambda_2^2\lambda_3^2 \end{aligned} \tag{5}$$

The polymers similar to liquids can move relative to one another, so that the rubber is easy to change shape. Given this molecular picture, it is clear that the rubber is much easier to change shape than change volume. The shear modulus is much smaller than the bulk modulus. In modeling, we often neglect the change in volume, and focus on change in shape. That is, we assume that the rubber is incompressible. Numerous polymeric materials can undergo finite strains without considerable volume changes. Such materials may be regarded as incompressible so that only isochoric motions are possible. For many cases, this is an idealization and the constraint $I_3=1$ is applied to the strain energy density function of these materials.

For the case of isotropy, the dependence of the strain energy density function on the Cauchy-Green tensors $\mathbf{C}$ or $\mathbf{B}$ may be expressed by their three strain invariants. However, for the incompressible case the two principal invariants I_1 and I_2 are the only independent deformation variables. A suitable strain-energy function for incompressible isotropic hyperelastic materials is in the form of[2]

$$W=W(I_1(\boldsymbol{B}),I_2(\boldsymbol{B}))-\frac{1}{2}p(I_3-1) \tag{6}$$

where W is the strain energy density function and p is the indeterminate scalar arising from the constraint of incompressibility.

The response of an incompressible isotropic elastic material can be derived based on eq. (6) in the following form (see, e.g., Truesdell and Noll,[17] Ogden,[1] and Beatty[18]):

$$\sigma=-p\boldsymbol{I}+2\frac{\partial W}{\partial I_1}\boldsymbol{B}-2\frac{\partial W}{\partial I_2}\boldsymbol{B}^{-1} \tag{7}$$

where σ denotes the Cauchy stress tensor. This standard constitutive law plays an important role in finite elasticity.

Constitutive Modeling

Several strain energy density expressions have been suggested for rubber. Darijani and Naghdabadi[19] used the phenomenological approach due to its relative simplicity and consistency within a continuum framework, to obtain the suitable forms for strain energy density function. They showed that a strain energy function for incompressible materials could be expressed as follows

$$W=w(\lambda_1)+w(\lambda_2)+w(\lambda_3) \tag{8}$$

where $w(\lambda_i)$ is the sum of the series as

$$w(\lambda_i)=\sum_{k=1}^{\infty}A_k(\lambda_i^{m_k}-1)+\sum_{k=1}^{\infty}B_k(\lambda_i^{-n_k}-1) \tag{9}$$

where m_k,n_k take real positive values and the coefficients A_k and B_k are the material parameters. A strain energy density

function can be approximated as closely as desired by suitable choice of these forms containing a finite number of terms. The number of parameters required to define the strain energy density depends on the level of nonlinearity and state of loadings. This study is focused on the strain energy density function with simple mathematical form that its effectiveness is evaluated using the experimental observations and is applied to find an analytical solution for the problem of torsion and extension of solid circular cylinders in the field of nonlinear elasticity. Setting $m_2=2, n_2=0$ and $m_2=2, n_2=2$ into eq. (9) gives the Neo-Hookean and Moony-Rivlin strain energy density models, respectively. These models have simple mathematical forms as follows

- Neo-Hookean strain energy function

$$\begin{aligned} W(\lambda_1,\lambda_2,\lambda_3)&=A_2\left(\lambda_2^2+\lambda_2^2+\lambda_3^2-3\right)\\ W(I_1)&=A_2^{\mathrm{Neo}}(I_1-3)\end{aligned} \tag{10}$$

- Moony-Rivlin strain energy function

$$\begin{aligned} W(\lambda_1,\lambda_2,\lambda_3)&=A_2\left(\lambda_1^2+\lambda_2^2+\lambda_3^2-3\right)+B_2\left(\lambda_1^{-2}+\lambda_2^{-2}+\lambda_2^{-2}-3\right)\\ W(I_1,I_2)&=A_2^{\mathrm{MR}}(I_1-3)+B_2^{\mathrm{MR}}(I_2-3)\end{aligned} \tag{11}$$

Setting $m_2=2, m_4=4, m_6=6, n_2=2$ into eq. (9), gives

$$\begin{aligned} W(\lambda_1,\lambda_2,\lambda_3)&=A_2\left(\lambda_1^2+\lambda_2^2+\lambda_3^2-3\right)+B_2\left(\lambda_1^{-2}+\lambda_2^{-2}+\lambda_3^{-2}-3\right)\\ &+A_4\left(\lambda_1^4+\lambda_2^4+\lambda_3^4-3\right)+A_6\left(\lambda_1^6+\lambda_2^6+\lambda_3^6-3\right)\end{aligned} \tag{12}$$

For an incompressible material, $I_3=1$, we can write the following relations

$$\begin{aligned} \lambda_1^2+\lambda_2^2+\lambda_3^2&=I_1\\ \lambda_1^{-2}+\lambda_2^{-2}+\lambda_3^{-2}&=I_2\\ \lambda_1^4+\lambda_2^4+\lambda_3^4&=I_1^2-2I_2\\ \lambda_1^{-4}+\lambda_2^{-4}+\lambda_3^{-4}&=I_2^2-2I_1\\ \lambda_1^6+\lambda_2^6+\lambda_3^6&=I_1^3-3I_1I_2+3\\ \lambda_1^{-6}+\lambda_2^{-6}+\lambda_3^{-6}&=I_2^3-3I_1I_2+3\\ \lambda_1^8+\lambda_2^8+\lambda_3^8&=I_1^4-4I_1^2I_2-2I_2^2+4I_1\\ \lambda_1^{-8}+\lambda_2^{-8}+\lambda_3^{-8}&=I_2^4-4I_2^2I_1-2I_1^2+4I_2\end{aligned} \tag{13}$$

Hence, eq. (12) in terms of the principal invarients of Cauchy-Green strain tensor **B** can be written as follows

$$W(I_1,I_2)=A_2(I_1-3)+B_2(I_2-3)+A_4\left(I_1^2-2I_2-3\right)+A_6\left(I_1^3-3I_1I_2\right) \tag{14}$$

Equation (14) is a new reconstructed model in terms of (I_1, I_2). A generalized form for strain energy density function in terms of (I_1, I_2) can be obtained by setting powers $m_2=2$, $m_4=4, m_6=6, m_8=8, \ldots$ & $n_2=2, n_4=4, n_6=6, n_8=8, \ldots$ as follows

$$\begin{aligned} W(I_1,I_2)&=B_2(I_2-3)+B_4\left(I_2^2-2I_1-3\right)+B_6\left(I_2^3-3I_1I_2\right)\\ &+B_8\left(I_2^4-4I_2^2I_1-2I_1^2+4I_2\right)+.\\ &A_2(I_1-3)+A_4\left(I_1^2-2I_2-3\right)+A_6\left(I_1^3-3I_1I_2\right)\\ &+A_8\left(I_1^4-4I_1^2I_2-2I_2^2+4I_1\right)+.\end{aligned} \tag{15}$$

Rivlin[8] proposed that a strain energy density function for incompressible materials could be expressed as the sum of the series in the following form

$$W=\sum_{p=0}^{\infty}\sum_{q=0}^{\infty}C_{pq}(I_1-3)^p(I_2-3)^q \tag{16}$$

for $(q=0, p=1)$, eq. (16) is reduced to the Neo-Hookean model, for set of $(q=0, p=1), (p=0, q=1)$, is reduced to the Moony-Rivlin model and for set of $(q=0, p=1)$, $(p=0, q=1)$, $(p=1, q=1)$, and $(p=3, q=0)$, is reduced to a model that its structure and terms are similar to eq. (14), a model from the set of generalized form for strain energy functions given in eq. (15), as follows

$$W=C_{10}(I_1-3)+C_{01}(I_2-3)+C_{11}(I_1-3)(I_2-3)+C_{30}(I_1-3)^3 \tag{17}$$

The determination of material parameters and the evaluating effectiveness of these models is based on the correlation between the values of the strain energy density (rather than the stresses) cast from the theory and the test data.[19] The test data involve a state of pure homogeneous deformation that includes simple tension/compression, pure shear, and equi-biaxial tension tests.

For an incompressible material, the principal components of the Lagrangian stress, S_i, and the Cauchy stress, σ_i, are obtained from the strain energy density as follows[1]

$$S_i=\frac{\partial W}{\partial\lambda_i}-\frac{p}{\lambda_i},\ \sigma_i=\lambda_i\frac{\partial W}{\partial\lambda_i}-p,\ \lambda_1\lambda_2\lambda_3=1 \tag{18}$$

In simple tension/compression, we know that $\sigma_1=\sigma, \lambda_1=\lambda$, and $\sigma_2=\sigma_3=0$. For isotropy of the material, $\lambda_2, \lambda_3=\lambda^{-0.5}$ and the stress-deformation relations are combined to give[19]

$$\sigma=\lambda\frac{\mathrm{d}\tilde{W}}{\mathrm{d}\lambda},\qquad \tilde{W}=\int_1^{\lambda}\frac{\sigma}{\lambda}\,\mathrm{d}\lambda \tag{19}$$

where $\tilde{W}(\lambda)=W\left(\lambda,\lambda^{-0.5},\lambda^{-0.5}\right)$.

For pure shear deformation, $\lambda_3=1$ and we set $\lambda_1=\lambda$, $\lambda_2=\lambda^{-1}$ with $\sigma_1=\sigma$, $\sigma_2=0$. A nonvanishing stress σ_3 is required to maintain $\lambda_3=1$. Eliminating σ_3, it can be concluded that

$$\sigma=\lambda\frac{\mathrm{d}\tilde{W}}{\mathrm{d}\lambda},\qquad \tilde{W}=\int_1^{\lambda}\frac{\sigma}{\lambda}\mathrm{d}\lambda, \tag{20}$$

where $\tilde{W}(\lambda)=W\left(\lambda,\lambda^{-1},1\right)$.

In equibiaxial tension, we have $\sigma_1=\sigma_2=\sigma$ and $\sigma_3=0$ coupled with $\lambda_1=\lambda_2=\lambda$. Consequently, we have

$$\sigma=0.5\lambda\frac{\mathrm{d}\tilde{W}}{\mathrm{d}\lambda},\qquad \tilde{W}=2\int_1^{\lambda}\frac{\sigma}{\lambda}\mathrm{d}\lambda \tag{21}$$

where $\tilde{W}(\lambda)=W\left(\lambda,\lambda,\lambda^{-2}\right)$.

Mechanical Behavior Modeling of Rubber-Like Materials

In this section, behavior modeling of hyperelastic materials arranged in the range of S-shaped to J-shaped is studied. Treloar[5] tested an unfilled natural rubber (cross-linked with 8 parts of S) under simple tension, pure shear and equi-biaxial tension up to quite large values of the stretch λ (about 7.0 in simple tension). The curves of stress-stretch of this rubber in the

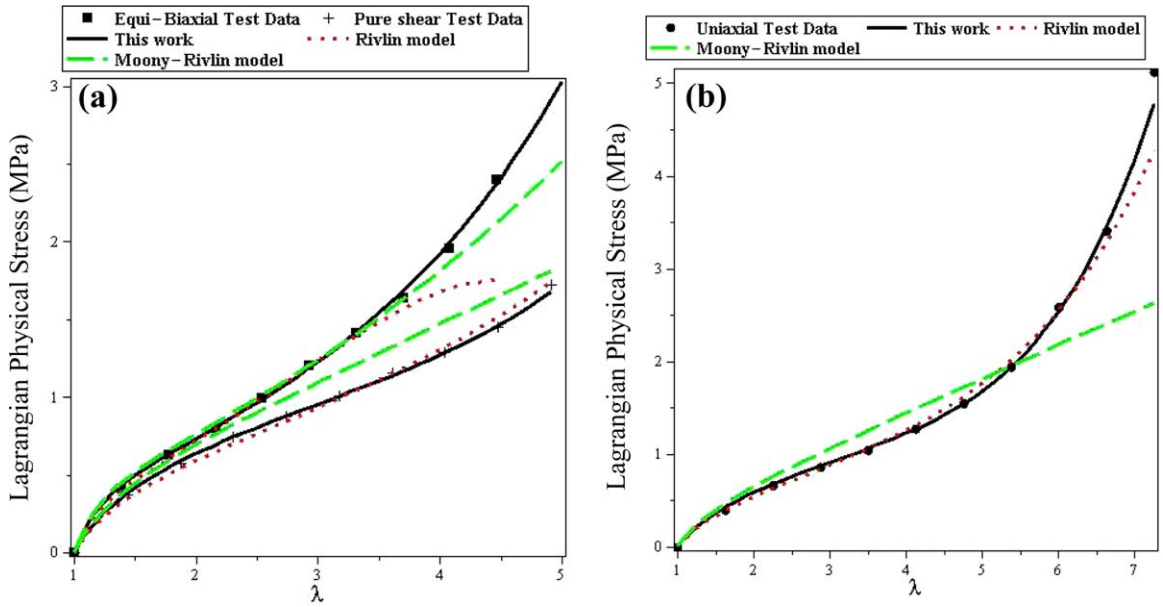

Figure 1. Comparison of the theory with the experimental results on the rubber of Treloar[5] (a) equi-biaxial and pure shear tests data and (b) uniaxial test data. [Color figure can be viewed in the online issue, which is available at wileyonlinelibrary.com.]

above-mentioned deformation modes is similar to S-shape (see Figure 1). Models of above-mentioned strain energy density with their descriptions for the test data are presented in Table I. The Table shows that the proposed model is more effective than the other models due to it has less residual sum of squares (RSS). Figure 1 depicts a comparison for the results of the theory and the tests on the rubber of Treloar. In addition, Figure 2 shows the errors of the strain energy models in fitting the test data of Treloar.[5]

Similarly, models of above-mentioned strain energy density with their descriptions for the test data of Alexander[20] and Heuillet and Dugautier[21] are presented in Tables II and III, respectively. Figures 3–5 show a comparison of the predictions for the stress values and those extracted from the experimental results of Alexander and Heuillet and Dugautier, respectively. In both Figures 3 and 5 there is a good agreement between the experimental and theoretical results. Figures 4 and 6 illustrate the estimated errors of the theoretical models in accordance with the test data of Alexander[20] and Heuillet and Dugautier,[21] respectively.

Table I. Evaluation Effectiveness of Models for Correlation with Test Data of Treloar[5]

Type of model	RSS	Material parameters
Proposed model	0.01	$A_2=0.3501/2, B_2=0.0109/2$ $A_4=-0.0064/4, A_6=0.0002/6$
Rivlin model	0.08	$C_{10}=0.1471, C_{01}=0.0097$ $C_{11}=-0.0002, C_{30}=0.00002$
Moony-Rivlin model	3.30	$A_2^{MR}=0.1812$ $B_2^{MR}=0.0028$
Neo-Hookean model	5.67	$A_2^{Neo}=0.1875$

In addition, Kawabata[22] tested a rubber under simple tension, pure shear, and equi-biaxial tension. Models of strain energy density mentioned above with their descriptions for the test data are presented in Table IV. The Table shows that the proposed model is more effective than the other models due to it has less RSS. Figure 7 depicts a comparison for the results of the theory and the tests on the rubber of Kawabata. The errors of the models are shown in Figure 8.

For the test data of Alexander, Rivlin model, eq. (17), has less RSS relative to the proposed model, eq. (14). However, for the other tests the proposed model show better agreement between the results of the theory and the test data.

Application

Energy function presented in this article is able to capture a wide range of mechanical behavior of hyperelastic materials from S-shaped to J-shaped. Thus, there is an expectation that applying these models for behavior prediction of a real structure gives dependable results. In this section using these energy functions, exact analytical solution without any simplification or forgoing part of solution can be achieved for a hyperelastic cylindrical tube under finite extension and torsion, steps to achieve the analytical solution is expressed very simple with the full details. In addition, these analytical solutions are physically appealing because they offer a clear view into how variables and interactions between variables affect the result, they have advantage of serving as a baseline reference for numerical solution and experimental results, analytical solutions are free from any error.

Finite Deformation of a Solid Cylinder Under Extension and Torsion

Consider a solid circular cylinder with radius A composed of an incompressible isotropic hyperelastic material subjected to a stretch in the axial direction and to a twist at its ends. The

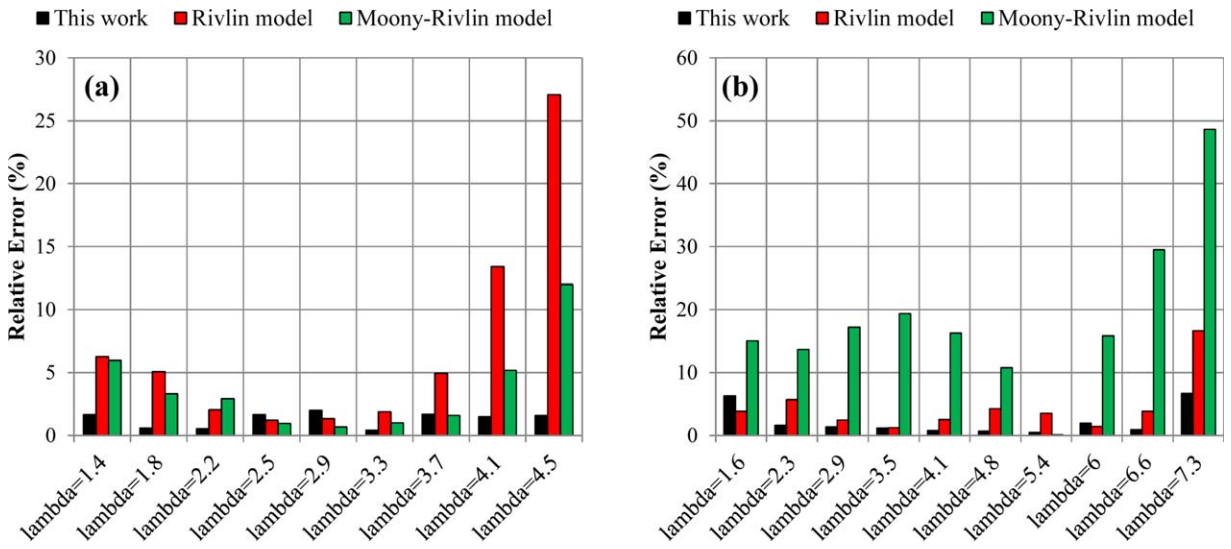

Figure 2. Estimation of error for the test data of Treloar[5] (a) equi-biaxial test data and (b) uniaxial test data. [Color figure can be viewed in the online issue, which is available at wileyonlinelibrary.com.]

cylindrical polar coordinates of a particle in the spatial and undeformed reference configurations are denoted by (r, θ, z) and (R, Θ, Z), respectively. The undeformed configuration of cylinder is

$$0 \le R \le A,\ 0 \le \Theta \le 2\pi,\ 0 \le Z \le L \tag{22}$$

Deformation of the cylinder is a pure torsion with plane cross sections remaining plane followed by a homogeneous extension or vice versa. Because of the symmetry of the geometry and loading conditions, the description of the material particles deformation in terms of current cylindrical polar coordinates (r, θ, z) is as follows[15]

$$r=\lambda^{-1/2}R,\ \theta=\Theta+\tau\lambda Z,\ z=\lambda Z \tag{23}$$

where τ is angle of twist per unit length of the current configuration and λ is the ratio of deformed length and the initial length L. The deformed radius a is given by $a=\lambda^{-1/2}A$. It is reasonable to expect that a stress system equivalent to a moment and an axial force is required to maintain the deformation. The physical components of the deformation gradient tensor $\boldsymbol{F}$ are

$$\boldsymbol{F}=\begin{bmatrix} \lambda^{-1/2} & 0 & 0 \\ 0 & \lambda^{-1/2} & \lambda^{1/2}R\tau \\ 0 & 0 & \lambda \end{bmatrix} \tag{24}$$

The left Cauchy-Green strain tensor $\boldsymbol{B}$ and its inverse are given by[15]

$$B=\begin{bmatrix} \lambda^{-1} & 0 & 0 \\ 0 & \lambda^{-1}+\lambda^2R^2\tau^2 & \lambda^{3/2}R\tau \\ 0 & \lambda^{3/2}R\tau & \lambda^2 \end{bmatrix},$$
$$B^{-1}=\begin{bmatrix} \lambda & 0 & 0 \\ 0 & \lambda & -\lambda^{1/2}\tau R \\ 0 & -\lambda^{1/2}\tau R & \lambda^{-2}+\tau^2R^2 \end{bmatrix} \tag{25}$$

The principal invariants of $\boldsymbol{B}$ are

$$\begin{aligned} I_1(R)&=\lambda^2+2\lambda^{-1}+\lambda\tau^2R^2 \\ I_2(R)&=2\lambda+\lambda^{-2}+\tau^2\mathrm{R}^2 \\ I_3&=1 \end{aligned} \tag{26}$$

Using eqs. (7) and (25), the nonzero components of the Cauchy stress tensor are as follows[15]

$$\sigma_r=-p+2\left\{\lambda^{-1}\frac{\partial W}{\partial I_1}-\lambda\frac{\partial W}{\partial I_2}\right\} \tag{27}$$

Table II. Evaluation Effectiveness of Models for Correlation with Test Data of Alexander[20]

Type of model	RSS	Material parameters
Proposed model	8.38	$A_2=0.2375/2, B_2=0.0828/2$
		$A_4=0.0279/4, A_6=0.0002/6$
Rivlin model	2.74	$C_{10}=0.3353, C_{01}=0.0141$
		$C_{11}=0.0002, C_{30}=0.0001$
Moony-Rivlin model	593.21	$A_2^{MR}=0.6457$
		$B_2^{MR}=0.0189$
Neo-Hookean model	1124.38	$A_2^{Neo}=0.7362$

Table III. Evaluation Effectiveness of Models for Correlation with Test Data of Heuillet and Dugautier[21]

Type of model	RSS	Material parameters
Proposed model	1.56	$A_2=0.5049/2, B_2=0.0346/2$
		$A_4=-0.0122/4, A_6=0.0003/6$
Rivlin model	2.09	$C_{10}=0.2062, C_{01}=0.0243$
		$C_{11}=-0.0002, C_{30}=-0.000004$
Moony-Rivlin model	2.34	$A_2^{MR}=0.2015$
		$B_2^{MR}=0.0216$
Neo-Hookean model	22.15	$A_2^{Neo}=0.2272$

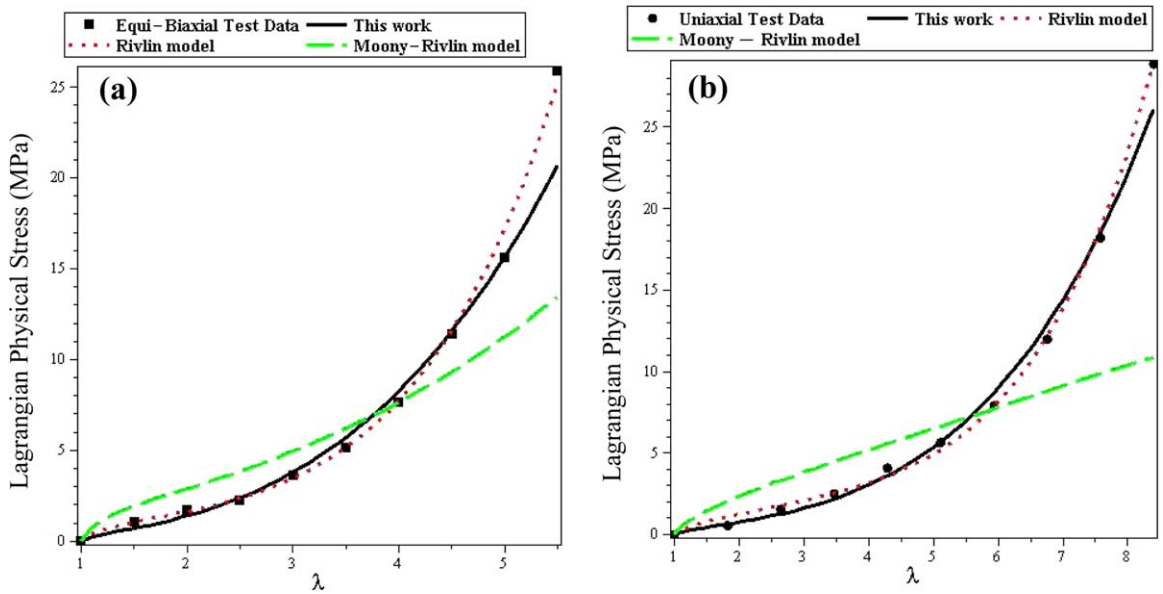

Figure 3. Comparison of the theoretical and experimental results on the neoprene film of Alexander[20] (a) equi-biaxial test data and (b) uniaxial test data. [Color figure can be viewed in the online issue, which is available at wileyonlinelibrary.com.]

$$\sigma_\theta = -p + 2\left\{(\lambda^{-1} + \lambda\tau^2 R^2)\frac{\partial W}{\partial I_1} - \lambda\frac{\partial W}{\partial I_2}\right\} \tag{28}$$

$$\sigma_z = -p + 2\left\{\lambda^2\frac{\partial W}{\partial I_1} - (\lambda^{-2} + \tau^2 R^2)\frac{\partial W}{\partial I_2}\right\} \tag{29}$$

$$\sigma_{\theta z} = 2\lambda^{1/2}\tau R\left\{\lambda\frac{\partial W}{\partial I_1} + \frac{\partial W}{\partial I_2}\right\} \tag{30}$$

The only nonzero trivial equilibrium equation is as follows

$$\frac{d\sigma_r}{dR} + \frac{\sigma_r - \sigma_\theta}{R} = 0 \tag{31}$$

Substituting eqs. (27) and (28) into eq. (31) gives

$$\frac{d\sigma_r}{dR} = -2\lambda\tau^2 R^2\frac{\partial W}{\partial I_1} \tag{32}$$

Solution of eq. (32) with boundry condition $\sigma_r(a)=0$, is in the form of

$$\sigma_r = \int_R^A -2\lambda\tau^2\frac{\partial W}{\partial I_1} RdR \tag{33}$$

Using eqs. (27) and (33), the scalar variable p is obtained and the other non-zero stresses become as follows[15,16]

$$\sigma_\theta = \int_R^A -2\lambda\tau^2\frac{\partial W}{\partial I_1} RdR + 2\lambda\tau^2 R^2\frac{\partial W}{\partial I_1} \tag{34}$$

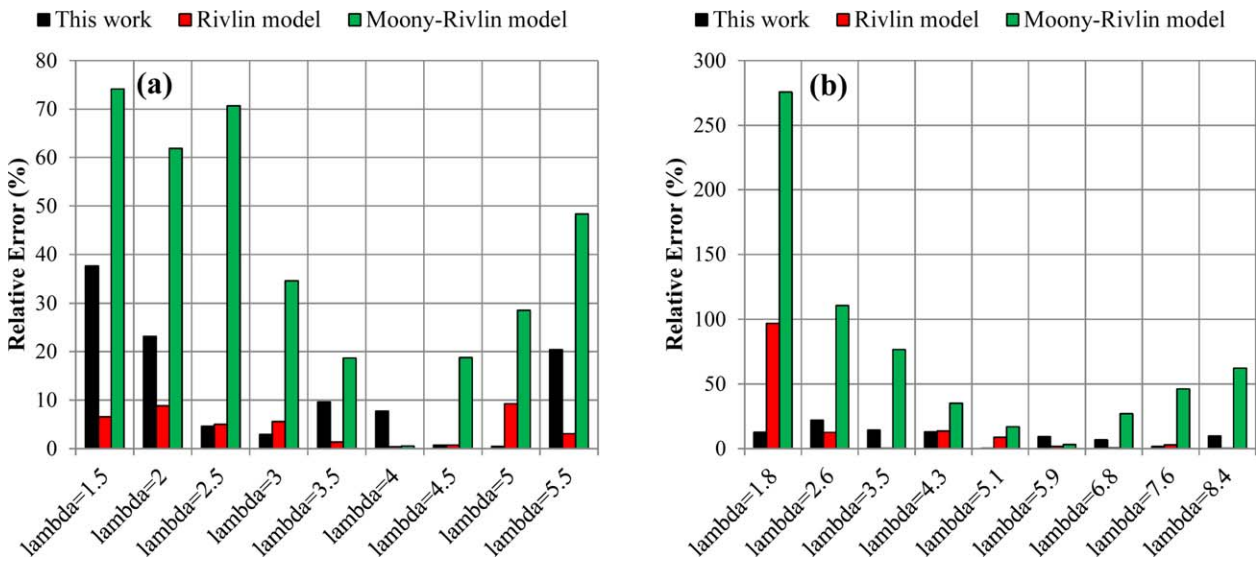

Figure 4. Estimation of error for the test data of Alexander[20] (a) equi-biaxial test data and (b) uniaxial test data. [Color figure can be viewed in the online issue, which is available at wileyonlinelibrary.com.]

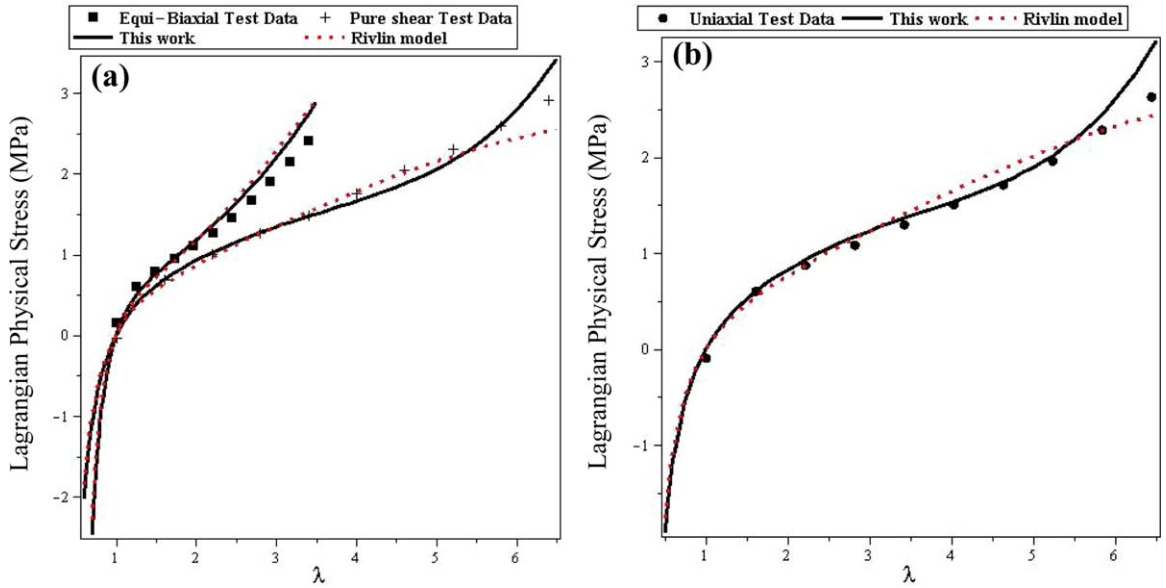

Figure 5. Comparison of the theoretical and experimental results on the rubber of Heuillet and Dugautier[21] (a) equi-biaxial and pure shear tests data and (b) uniaxial test data. [Color figure can be viewed in the online issue, which is available at wileyonlinelibrary.com.]

$$\sigma_z=\int_R^A -2\lambda\tau^2\frac{\partial W}{\partial I_1}RdR+2(\lambda^2-\lambda^{-1})\frac{\partial W}{\partial I_1}+2(\lambda-\lambda^{-2}-\tau^2R^2)\frac{\partial W}{\partial I_2} \tag{35}$$

$$\sigma_{\theta z}=2\lambda^{3/2}\tau R\frac{\partial W}{\partial I_1}+2\lambda^{1/2}\tau R\frac{\partial W}{\partial I_2} \tag{36}$$

The resultant applied moment M and axial force N required for maintaining the deformation are[15,16]

$$M=2\pi\int_0^A \sigma_{\theta z}r^2dr \tag{37}$$

$$N=2\pi\int_0^A \sigma_z rdr \tag{38}$$

substituting eqs. (35) and (36) into eqs. (37) and (38), we have

$$M=\int_0^A R^3\left(\frac{\partial W}{\partial I_1}+\lambda^{-1}\frac{\partial W}{\partial I_2}\right)dR \tag{39}$$

$$N=4\pi(\lambda-\lambda^{-2})\int_0^A R\left(\frac{\partial W}{\partial I_1}+\lambda^{-1}\frac{\partial W}{\partial I_2}\right)dR -2\pi\tau^2\int_0^A R^3\left(\frac{\partial W}{\partial I_1}+2\lambda^{-1}\frac{\partial W}{\partial I_2}\right)dR \tag{40}$$

Based on the Neo-Hookean, Moony-Rivlin and the proposed model, a closed-form solution is obtained for stresses, moment, and axial force as follows

- Neo-Hookean model

$$\sigma_r=-A_2^{\mathrm{Neo}}\lambda\tau^2(A^2-R^2) \tag{41}$$

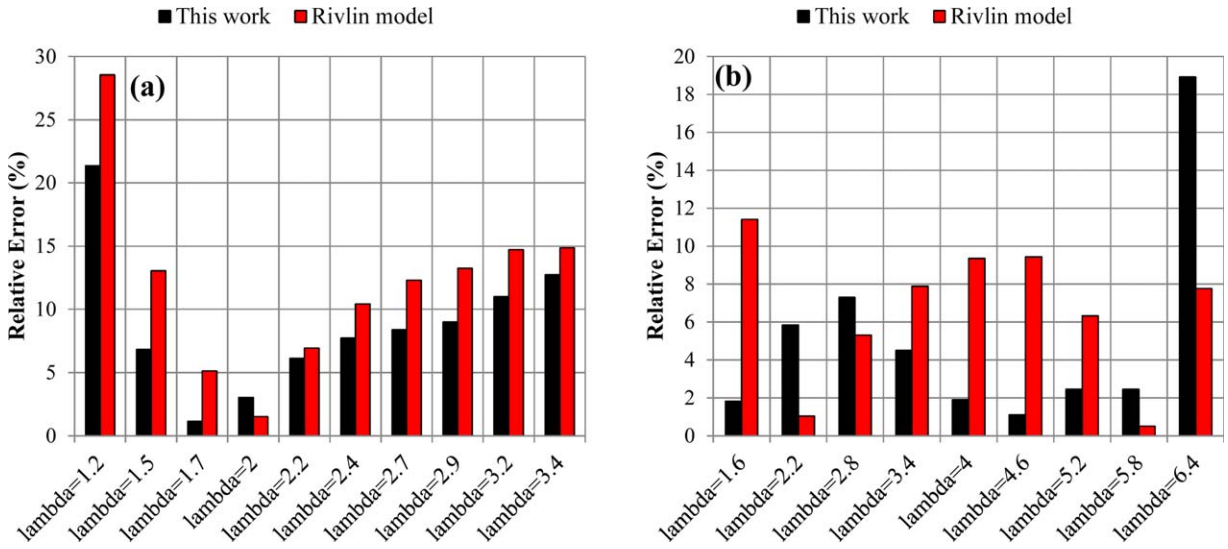

Figure 6. Estimation of error for the test data of Heuillet[21] (a) equi-biaxial test data and (b) uniaxial test data. [Color figure can be viewed in the online issue, which is available at wileyonlinelibrary.com.]

Table IV. Evaluation Effectiveness of Models for Correlation with Test Data of Kawabata[22]

Type of model	RSS	Material parameters
Proposed model	0.002	$A_2=0.4504/2, B_2=0.0115/2$
		$A_4=-0.0309/4, A_6=0.0015/6$
Rivlin model	0.007	$C_{10}=0.1654, C_{01}=0.0143$
		$C_{11}=-0.0003, C_{30}=-0.00009$
Moony-Rivlin model	0.064	$A_2^{MR}=0.1626$
		$B_2^{MR}=0.0074$
Neo-Hookean model	0.353	$A_2^{Neo}=0.1824$

$$\sigma_\theta=-A_2^{Neo}\lambda\tau^2(A^2-3R^2) \tag{42}$$

$$\sigma_z=A_2^{Neo}\left[-\lambda\tau^2(A^2-R^2)+2(\lambda^2-\lambda^{-1})\right] \tag{43}$$

$$\sigma_{\theta z}=2A_2^{Neo}\lambda^{3/2}\tau R \tag{44}$$

$$M=A_2^{Neo}\pi\tau A^4 \tag{45}$$

$$N=2A_2^{Neo}\pi A^2\left(\lambda-\lambda^{-2}-\frac{\tau^2A^2}{4}\right) \tag{46}$$

- Moony-Rivlin model

$$\sigma_r=-A_2^{MR}\lambda\tau^2(A^2-R^2) \tag{47}$$

$$\sigma_\theta=-A_2^{MR}\lambda\tau^2(A^2-3R^2) \tag{48}$$

$$\sigma_z=A_2^{MR}\left[-\lambda\tau^2(A^2-R^2)+2\ (\lambda^2-\lambda^{-1})\right]+2B_2^{MR}\left(\lambda-\lambda^{-2}-\tau^2R^2\right) \tag{49}$$

$$\sigma_{\theta z}=2\lambda^{1/2}\tau R(\lambda A_2^{MR}+B_2^{MR}) \tag{50}$$

$$M=\pi\tau A^4(A_2^{MR}+\lambda^{-1}B_2^{MR}) \tag{51}$$

$$N=2\pi A^2\left[(\lambda-\lambda^{-2})(A_2^{MR}+\lambda^{-1}B_2^{MR})-\frac{\tau^2A^2}{4}(A_2^{MR}+2\lambda^{-1}B_2^{MR})\right] \tag{52}$$

- Proposed model

$$\sigma_r=f[I_1(A)]-f[I_1(R)] \tag{53}$$

$$\sigma_\theta=f[I_1(A)]-f[I_1(R)]+2\lambda\tau^2R^2\{A_2^O+2A_4^OI_1(R)+3A_6^O[(I_1(R))^2-I_2(R)]\} \tag{54}$$

$$\sigma_z=f[I_1(A)]-f[I_1(R)]+2(\lambda^2-\lambda^{-1})[A_2^O+2A_4^OI_1(R)+3A_6^O((I_1(R))^2-I_2(R))]+2(\lambda-\lambda^{-2}-\tau^2R^2)[B_2^O-2A_4^O-3A_6^OI_1(R)] \tag{55}$$

$$\sigma_{\theta z}=2\lambda^{3/2}\tau R[A_2^O+2A_4^OI_1(R)+3A_6^O((I_1(R))^2-I_2(R))]+2\lambda^{1/2}\tau R[B_2^O-2A_4^O-3A_6^OI_1(R)] \tag{56}$$

$$M=\frac{2\pi}{\lambda^2\tau^3}\{g(I_1(A))-g(I_1(0))\} \tag{57}$$

$$N=\frac{2\pi(1-\lambda^{-3})}{\tau^2}\{h_1(I_1(A))-h_1(I_1(0))\}-\frac{\pi}{\lambda^2\tau^2}\{h_2(I_1(A))-h_2(I_1(0))\} \tag{58}$$

where

$$f=[3(\lambda-\lambda^{-2})A_6^O-A_2^O]I_1+\frac{1}{2}[3\lambda^{-1}A_6^O-2A_4^O]I_1^2-A_6^OI_1^3 \tag{59}$$

$$g=[-(\lambda^2+2\lambda^{-1})A_2^O-(\lambda+2\lambda^{-2})B_2^O+2(\lambda+2\lambda^{-2})A_4^O+3(1-\lambda^{-3})A_6^O]I_1+\frac{1}{2}[A_2^O+\lambda^{-1}B_2^O-2(\lambda^2+3\lambda^{-1})A_4^O+3(5\lambda^{-2}+\lambda)A_6^O]I_1^2+\frac{1}{3}[2A_4^O-3(\lambda^2+4\lambda^{-1})A_6^O]I_1^3+\frac{3}{4}A_6^OI_1^4 \tag{60}$$

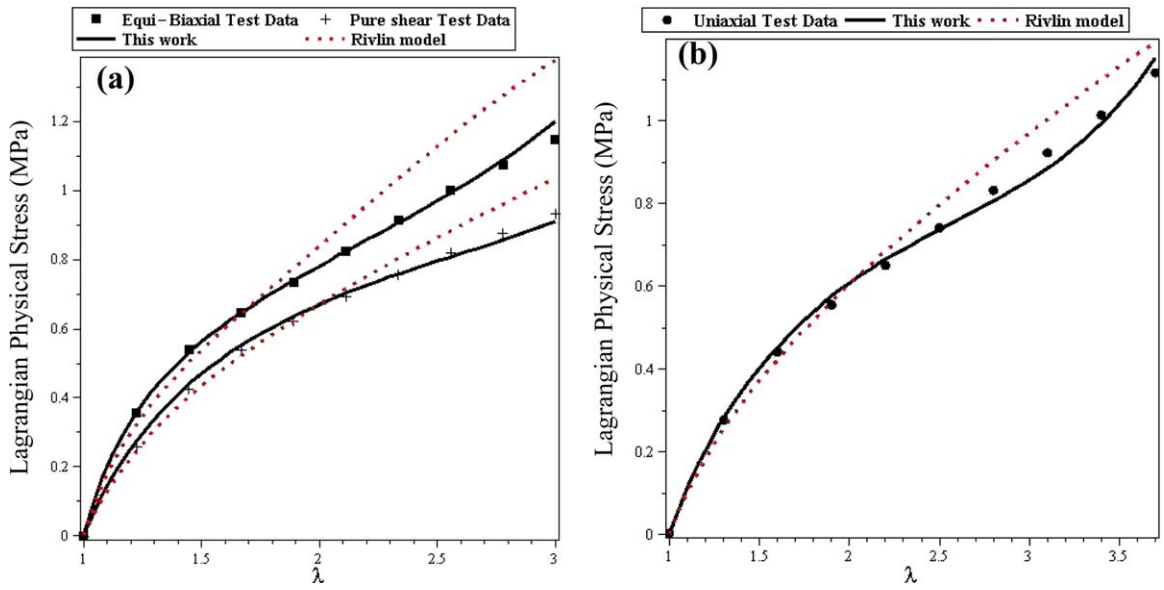

Figure 7. Comparison of the theory with the experimental results on the rubber of Kawabata[22] (a) equi-biaxial and pure shear tests data and (b) uniaxial test data. [Color figure can be viewed in the online issue, which is available at wileyonlinelibrary.com.]

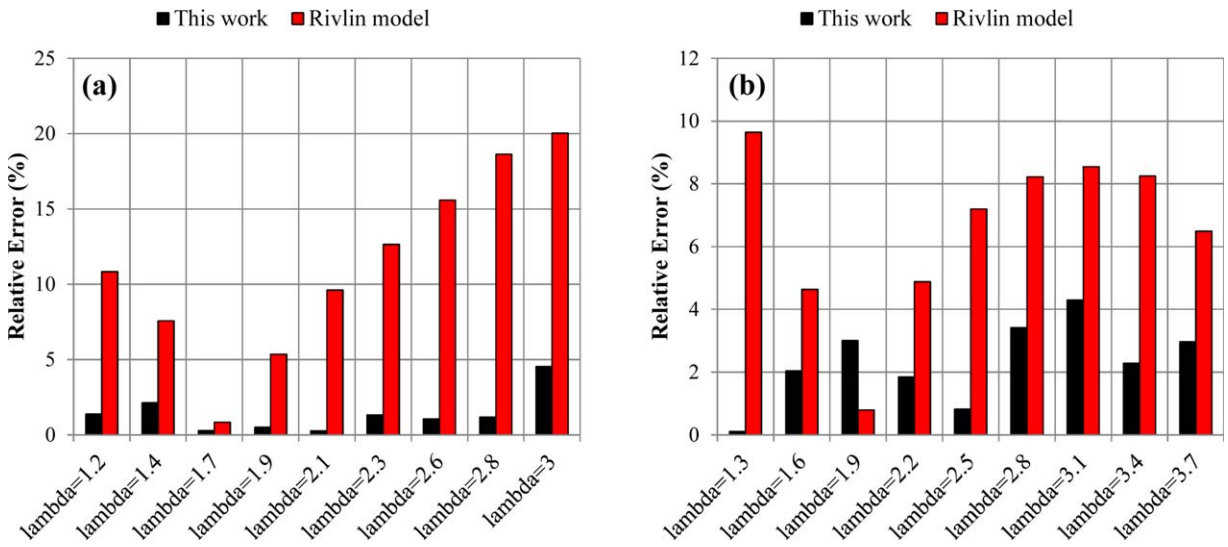

Figure 8. Estimation of error for the test data of Kawabata[22] (a) equi-biaxial test data and (b) uniaxial test data. [Color figure can be viewed in the online issue, which is available at wileyonlinelibrary.com.]

$$h_1=[A_2^O+\lambda^{-1}B_2^O-2\lambda^{-1}A_4^O-3(\lambda-\lambda^{-2})A_6^O] \\ I_1+[A_4^O-3\lambda^{-1}A_6^O]I_1^2+A_6^OI_1^3 \tag{61}$$

$$h_2=[-(\lambda^2+2\lambda^{-1})A_2^O-2(\lambda+2\lambda^{-2})B_2^O+4(\lambda+2\lambda^{-2})A_4^O \\ +3(1-\lambda^{-3})A_6^O]I_1+\frac{1}{2}[A_2^O+2\lambda^{-1}B_2^O-2(\lambda^2+4\lambda^{-1})A_4^O \\ +3(7\lambda^{-2}+2\lambda)A_6^O]I_1^2+\frac{1}{3}[2A_4^O-3(5\lambda^{-1}+\lambda^2)A_6^O]I_1^3+\frac{3}{4}A_6^OI_1^4 \tag{62}$$

Pure Torsion

If we set $\lambda=1$ in the preceding, one recovers the problem of pure torsion. From eq. (26), we have[15]

$$I_1(r)=I_2(r)=3+\tau^2r^2,\ I_3=1 \tag{63}$$

Since $r=R$ For simple torsion, we can write all equations in terms of r. Also, the undeformed and the current radius of the cylinder are denoted as a. We obtain the results of stresses, moment, and axial force for the problem of pure torsion extracted from the proposed model as follows

$$\sigma_r=f(I_1(a))-f(I_1(r)) \tag{64}$$

$$\sigma_\theta=f(I_1(a))-f(I_1(r))+2\tau^2r^2[A_2^O+2A_4^OI_1(r) \\ +3A_6^O((I_1(r))^2-I_2(r))] \tag{65}$$

$$\sigma_z=f(I_1(a))-f(I_1(r))-2\tau^2r^2[B_2^O-2A_4^O-3A_6^OI_1(r)] \tag{66}$$

$$\sigma_{\theta z}=2\tau r[A_2^O+B_2^O+2A_4^O(I_1(r)-1)+3A_6^O((I_1(r))^2-I_1(r)-I_2(r))] \tag{67}$$

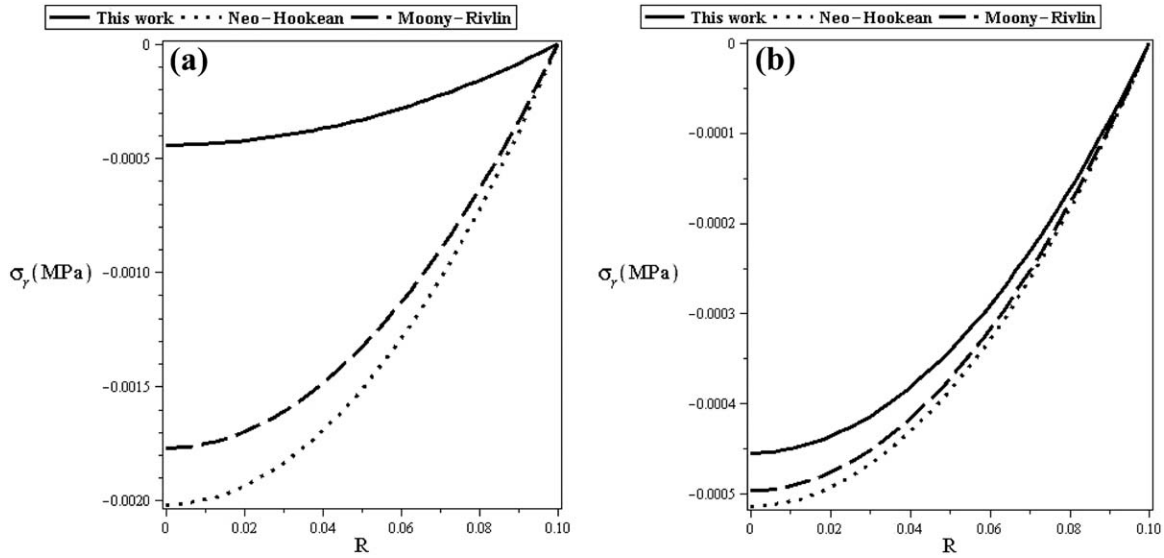

Figure 9. Radial stress σ_r versus R for (a) a solid RA cylinder (b) a solid RT cylinder when $A=0.1$ m, $\tau=\pi/6$ rad/m and $\lambda=1$.

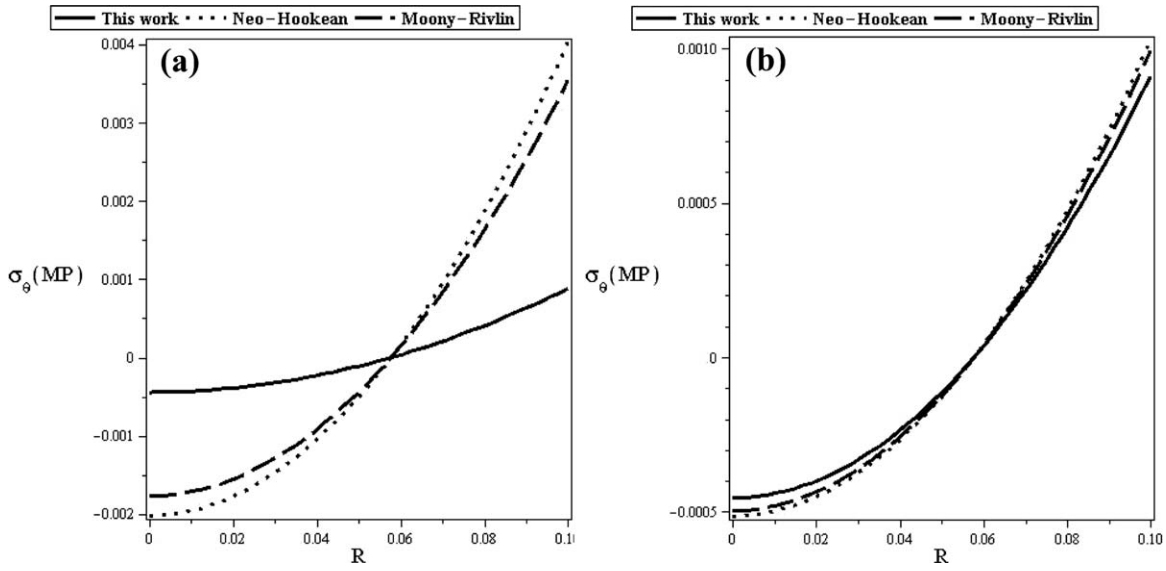

Figure 10. Hoop stress σ_θ versus R for (a) a solid RA cylinder (b) a solid RT cylinder when $A = 0.1$ m, $\tau = \pi/6$ rad/m and $\lambda = 1$.

$$M = \frac{2\pi}{\tau^3}\{g(I_1(a)) - g(I_1(0))\} \tag{68}$$

$$N = -\frac{\pi}{\tau^2}\{h(I_1(a)) - h(I_1(0))\} \tag{69}$$

where

$$f = -A_2^O I_1 + \frac{1}{2}[3A_6^O - 2A_4^O]I_1^2 - A_6^O I_1^3 \tag{70}$$

$$g = [-3A_2^O - 3B_2^O + 6A_4^O]I_1 + \frac{1}{2}[A_2^O + B_2^O - 8A_4^O + 18A_6^O]I_1^2 + \frac{1}{3}[2A_4^O - 15A_6^O]I_1^3 + \frac{3}{4}A_6^O I_1^4 \tag{71}$$

$$h = [-3A_2^O - 6B_2^O + 12A_4^O]I_1 + \frac{1}{2}[A_2^O + 2B_2^O - 10A_4^O + 27A_6^O] I_1^2 + \frac{1}{3}[2A_4^O - 18A_6^O]I_1^3 + \frac{3}{4}A_6^O I_1^4 \tag{72}$$

RESULTS AND DISCUSSIONS

There has been remarkable interest to know that how an appropriate strain energy density is selected for response prediction of a structure which undergoes 3D deformations. It can be claimed that difference among the results predicted based on different strain energy models depends on the degree of their correlation with test data. Figure 1 shows that Neo-Hookean

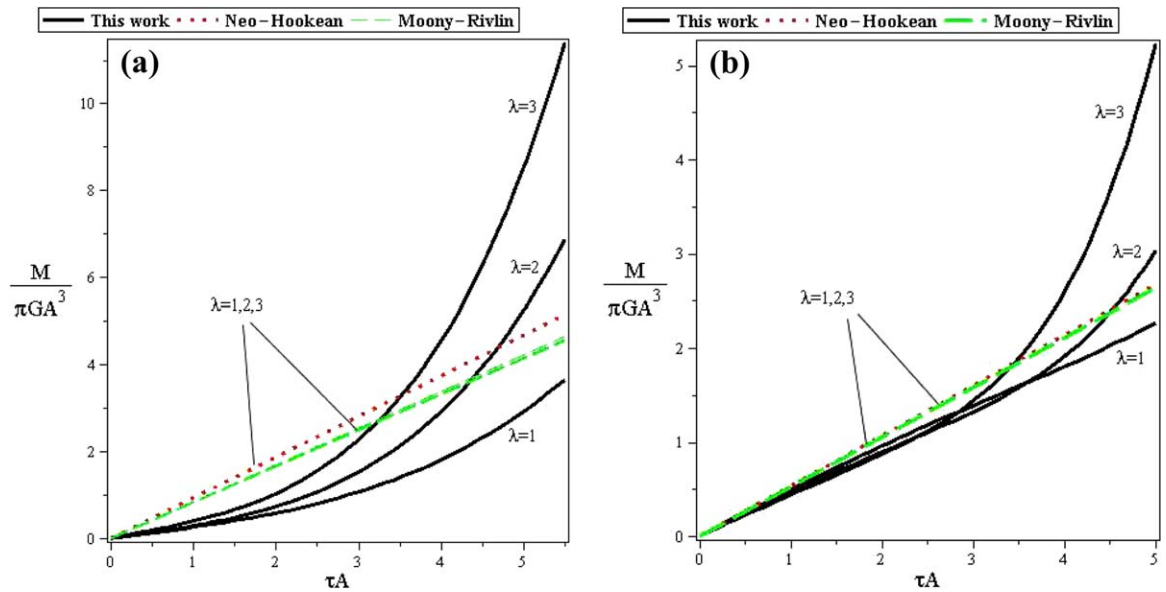

Figure 11. Nondimensional applied moment versus total angle of twist τA for (a) a solid RA cylinder (b) a solid RT cylinder. [Color figure can be viewed in the online issue, which is available at wileyonlinelibrary.com.]

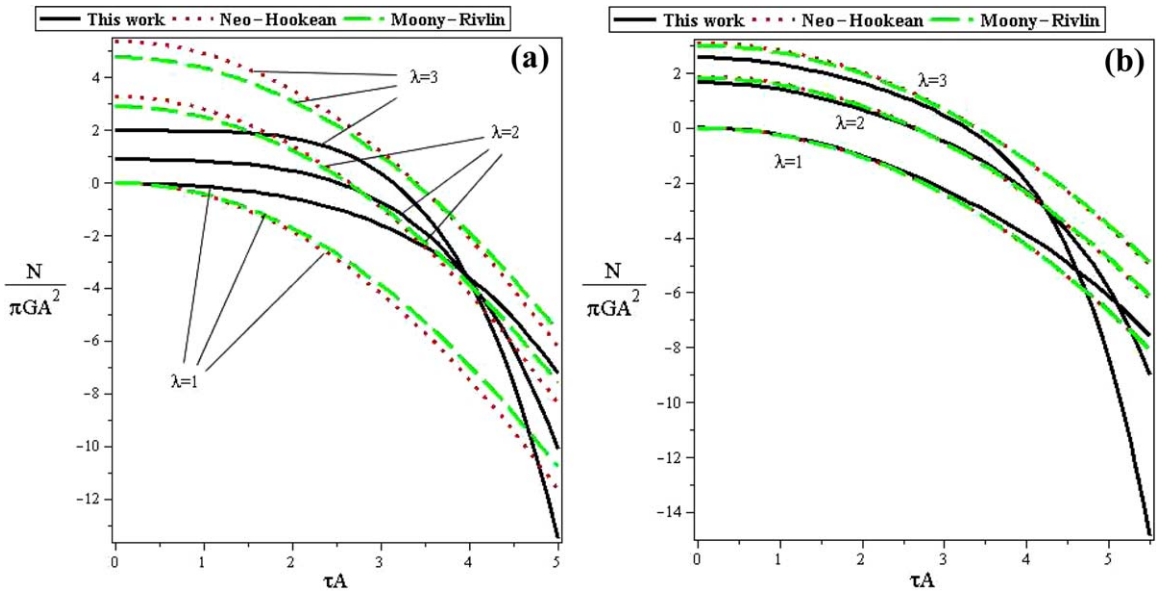

Figure 12. Nondimensional resultant axial force versus total angle of twist τA for (a) a solid RA cylinder (b) a solid RT cylinder. [Color figure can be viewed in the online issue, which is available at wileyonlinelibrary.com.]

and Mooney-Rivlin models can follow the test data of the rubber tested by Treloar for stretches <2. It seems that these models are able to capture S-shaped mechanical behavior of the materials with moderate deformations. It can be expected that applying Neo-Hookean and Mooney-Rivlin models to a real structure made of the rubber tested by Treloar under moderate deformations can yield acceptable results. In Figure 3, the correlation of Neo-Hookean and Mooney-Rivlin with the test data of the rubber tested by Alexander shows that these models cannot follow the material behavior. It seems that Neo-Hookean and Mooney-Rivlin models are not able to track the trend of semi J-shaped mechanical behavior of the materials. Thus, there is an expectation that applying Neo-Hookean and Mooney-Rivlin for behavior prediction of a real RA structure, made of the rubber tested by Alexander, gives undependable results. In the following, Figures 9–12 confirm the above-mentioned comments.

In addition, we expect the trend and the values of the results obtained from the presented strain energy to be comparable with experimental observations. In fact, to compare the analytical solutions obtained with their corresponding experimental data, we need the test data related to the cylindrical tubes made of RT (the rubber tested by Treloar) and RA (the rubber tested by Alexander). Since there is no available test data related to this problem, we can only compare the results from the proposed model with those extracted from the classic models.

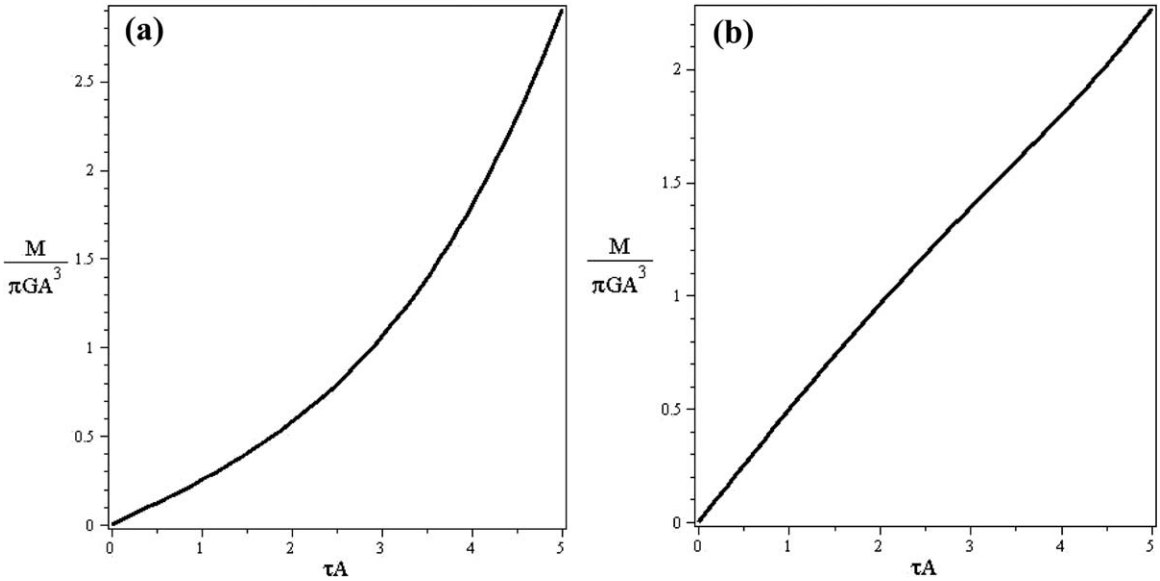

Figure 13. Nondimensional applied moment versus total angle of twist τA in the pure torsion for (a) a solid RA cylinder (b) a solid RT cylinder.

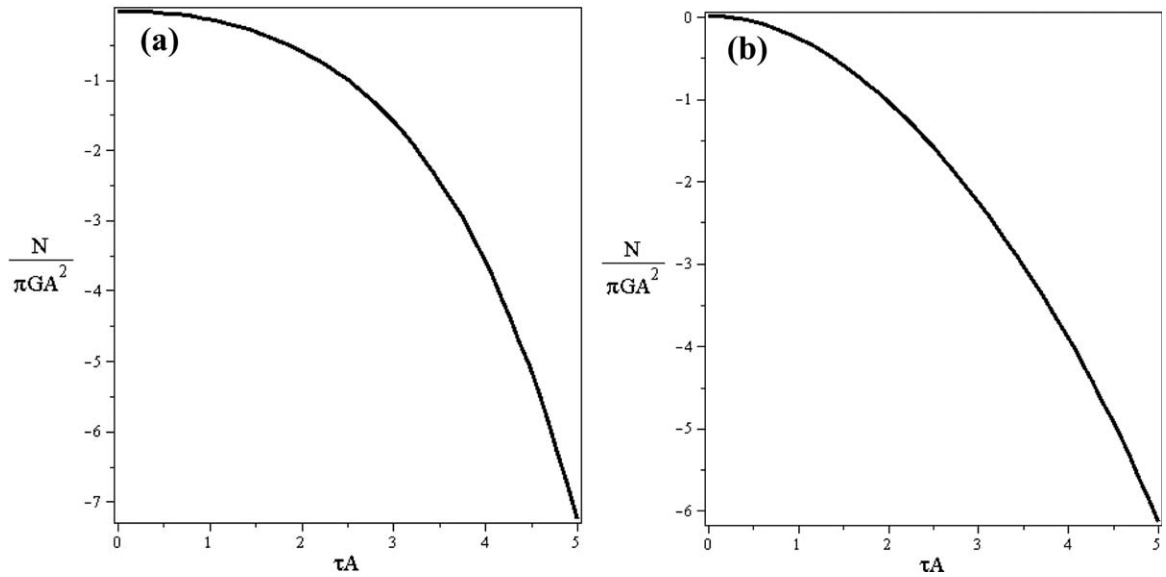

Figure 14. Nondimensional resultant axial force versus total angle of twist τA in the pure torsion for (a) a solid RA cylinder (b) a solid RT cylinder.

Figure 9(a,b) show the distribution of radial stress, σ_r, predicted from the proposed model and two classical models for a solid cylinder made of the material tested by Alexander (which is called solid RA cylinder in the following) and a solid cylinder made of the rubber tested by Treloar (which is called solid RT cylinder in the following), respectively. Also, Figure 10(a,b) show the distribution of hoop stress, σ_θ, predicted from the proposed model and two classical models for a solid RA cylinder and a solid RT cylinder, respectively.

As it can be seen from Figures 9 and 10, the difference between the results predicted from the proposed model and the classic models for the solid RA cylinder is significant while this difference for the solid RT cylinder is negligible.

In Figures 11 and 12, we plot the nondimensional applied moment and axial force versus total angle of twist τA for a solid circular cylinder under torsion and extension. As it can be seen from these figures, for a solid RA cylinder under torsion and extension the results obtained from the proposed model and two other classic models are not coincident and their difference is considerable. While, for a solid RT cylinder under torsion and extension the results predicted from the proposed model and two other classic models are almost coincident till angle of twist $\tau A=1.5$. This angel of twist for solid circular RT cylinder is corresponded to limit point of the moderate deformations. Since the proposed model has less RSSs it can be concluded that the results predicted from this model is more accurate than classic models. Since that difference between the results extracted from the models of strain energy depends on the degree of their agreement to the test data (see RSS given in Tables I and II), the curves related to Neo-Hookean and Moony-Rivlin models are almost coincident together in Figures 11 and 12.

Thus, Moony-Rivlin and Neo-Hookean are reasonably accurate in predicting the response of the solid circular RT cylinder under extension and torsion at small ranges of stretch whereas for larger values of stretch, they fail to predict the strain-stiffening that is observed experimentally.

These models are not able to predict the response of a solid circular cylinder made of the materials with strain-stiffening behavior. As it can be seen from Figure 12, regardless of the amount of stretch λ, the axial force increases as τA increases. Hence, using the proposed model, resultant axial force necessary to maintain deformation is compressive such that in the absence of this force, the cylinder always has a tendency to elongate upon twisting.

In Figures 13 and 14, we plot the nondimensional applied moment and axial force versus total angle of twist τA for a solid

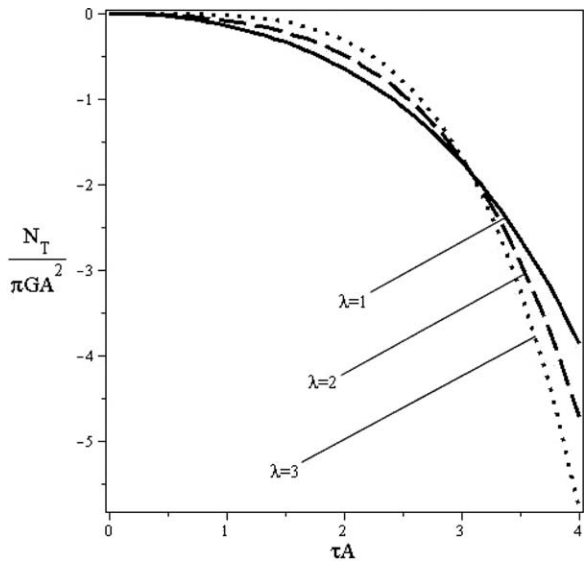

Figure 15. Nondimensional additional axial force versus total angle of twist τA for a solid RA cylinder.

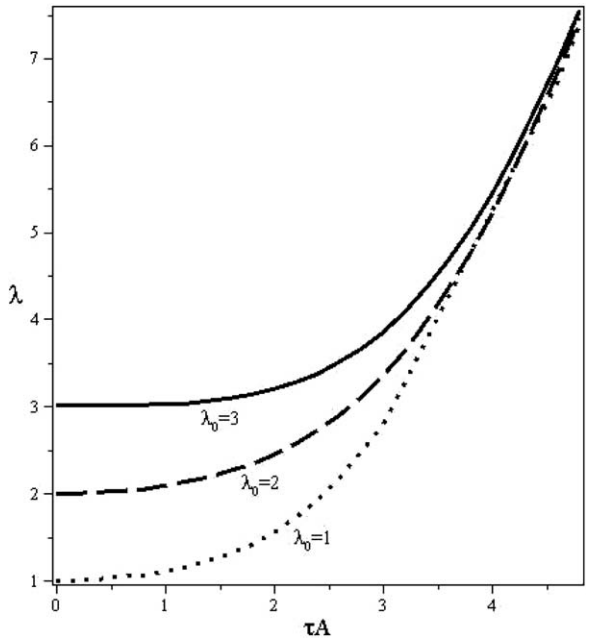

Figure 16. Stretch λ versus τA for various nondimensional values of $N_0 = 0, 0.9, 2$ corresponding to $\lambda_0 = 1, 2, 3$.

circular cylinder under pure torsion predicted by the proposed model. It can be verified that the resultant axial force, N, required to maintain pure torsion is compressive. In the absence of such a force, the bar would elongate on twisting reflecting the celebrated Poynting effect.[23] To investigate the dependence of the resultant moment M and axial force N on the twist τ and the stretch λ, we define $N_0 \equiv N(\lambda=\lambda_0, \tau=0)$, in fact $N_0(\lambda_0)$ is the axial force necessary to produce an axial stretch $\lambda=\lambda_0$ in the absence of twist. N_T is defined as follows[15]

$$N(\lambda_0, \tau) = N_0(\lambda_0) + N_T(\lambda_0, \tau) \tag{73}$$

N_T is an additional axial force that is necessary to maintain a constant stretch of $\lambda=\lambda_0$ under torsion. From eq. (40) we have

$$N_0(\lambda_0) = 2\pi A^2 \left(\lambda_0 - \lambda_0^{-2}\right)\left(\frac{\partial W}{\partial I_1} + \lambda_0^{-1}\frac{\partial W}{\partial I_2}\right) \tag{74}$$

Using eqs. (40), (73), and (74), an expression for $N_T$is yielded. In the absence of the additional force N_T, the stretch λ under torsion differs from λ_0. If N is an increasing function of τ, N_T is positive and if N is a decreasing function of τ, N_T is negative. In Figure 15, the nondimensional additional axial force is plotted versus total angle of twist τA predicted from the proposed model.

Figure 15 shows that the additional axial force for maintaining a constant axial stretch is always compressive. In the absence of such a force, the cylinder tends to elongate under torsion. We can consider a constant axial force N to know that how λ changes as a function of τ rather than keeping the stretch constant. If we assume[15]

$$N(\lambda, \tau) = N_0(\lambda_0, \tau=0) \tag{75}$$

Then for an arbitrary λ_0, we can obtain from eq. (75), $\lambda=\lambda(\tau)$. In Figure 16, we plot λ versus τA when $N=N_0(\lambda_0)$ for $\lambda_0 = 1, 2, 3$ predicted from the proposed model. It is clear that each curve in Figure 16 intercepts the vertical axis at $\lambda=\lambda_0$. The values N_0 may be calculated from eq. (74) and depend on the constitutive model being used. Value $N_0=0$ corresponds to $\lambda_0=1$.

CONCLUSION

In this article, the focus was on modeling mechanical behavior of a class of incompressible materials using the polynomial models of strain energy density. A polynomial strain energy density function in terms of the principal invariants of Cauchy-Green strain tensor **B** has been proposed and compared with a similar function form the set of Rivlin. The appropriateness of the proposed model for describing the high deformability of rubber-like materials in large strain levels has been investigated using several tests. The results show the good agreement between the experimental findings and theoretical predictions from the proposed model. As an application of the proposed model, it has been used to obtain a closed-form solution for the stress analysis of the rubbery solid circular cylinders made of the elastomers with S-shaped and semi J-shaped mechanical behavior under simultaneous torsion and extension. The results obtained from the classical models (Neo-Hookean and Moony-Rivlin) and the proposed model show a significant difference for solid circular cylinders made of the materials with semi J-shaped behavior while this difference is negligible for materials with S-shaped behavior. Moreover, it was observed that the resultant axial force necessary to maintain deformation is compressive such that in the absence of such an axial force, the cylinders tend to elongate on both pure torsion and simultaneous extension and torsion cases.

REFERENCES

1. Ogden, R. W. Non-Linear Elastic Deformations; Dover Publications: Mineola, **1997**.
2. Holzapfel, G. A. Nonlinear Solid Mechanics; Wiley: Chichester, **2001**.
3. Steinmann, P.; Hossain, M.; Possart, G. *Arc. Appl. Mech.* **2012**, *82*, 1183.
4. Mooney, M. *J. Appl. Phys.* **1940**, *11*, 582.
5. Treloar, L. R. G. *Trans. Faraday Soc.* **1944**, *40*, 59.
6. Kakavas, P. A. *J. Appl. Polym. Sci.* **2000**, *77*, 660.
7. Gent, A. N. *Rubber Chem. Technol.* **1996**, *69*, 59.
8. Rivlin, R. S. *Philos. Trans. R. Soc. A* **1948**, *240*, 459.
9. Yeoh, O. H. *Rubber Chem. Technol.* **1993**, *66*, 754.
10. Biderman, V. L. Calculation of Rubber Parts; Rascheti na Prochnost: Moscow, **1958**.
11. Rivlin, R. S.; Saunders, D. W. *Philos. Trans. R. Soc. A* **1951**, *243*, 251.
12. Valanis, K. C.; Landel, R. F. *J. Appl. Phys.* **1967**, *38*, 2997.
13. Attard, M. M. *Int. J. Solids Struct.* **2003**, *40*, 4353.
14. Ogden, R. W. *J. Phys. D: Appl. Phys.* **1979**, *12*, 1463.
15. Kanner, L. M.; Horgan, C. O. *J. Elast.* **2008**, *93*, 39.
16. Horgan, C. O.; Murphy, J. G. *J. Elast.* **2011**, *16*, 482.
17. Truesdell, C.; Noll, W. The Nonlinear Field Theories of Mechanics; Antman, S. S., Ed.; Springer: Berlin, **2004**.

18. Beatty, M. F. *Appl. Mech. Rev.* **1987**, *40*, 1699.
19. Darijani, H.; Naghdabadi, R. *Acta Mech.* **2010**, *213*, 235.
20. Alexander, H. *Int. J. Eng. Sci.* **1968**, *9*, 549.
21. Heuillet, P.; Dugautier, L. Modelisation du comportement hyperelastique des caoutchoucs et elastomeres thermoplastiques, compacts on cellulaires. Genie Mecanique des Caoutchoucs et des Elastomeres Thermoplastiques **1997**.
22. Kawabata, S.; Matsuda, M.; Tel, K.; Kawai, H. *Macromolecules* **1981**, *14*, 154.
23. Poynting, J. H. *Proc. R. Soc. Lond. A* **1912**, *86*, 534.